



Conjugated microporous poly(benzothiadiazole)/TiO₂ heterojunction for visible-light-driven H₂ production and pollutant removal



Hui-Jie Hou^{a,1}, Xiao-Hu Zhang^{a,1}, De-Kang Huang^a, Xing Ding^a, Sheng-Yao Wang^{a,b}, Xiang-Long Yang^a, Sheng-Qing Li^a, Yong-Gang Xiang^{a,*}, Hao Chen^{a,b,**}

^a College of Science, Huazhong Agricultural University, Wuhan 430070, PR China

^b Key laboratory of Environment Correlative Dietology, Ministry of Education, Wuhan 430070, PR China

ARTICLE INFO

Article history:

Received 25 August 2016

Received in revised form 7 October 2016

Accepted 20 October 2016

Available online 21 October 2016

Keywords:

Organic/inorganic semiconductors composite

Heterojunction

Photocatalytic H₂ production

Photocatalytic pollutant removal

Visible light response

ABSTRACT

A π-conjugated microporous poly(benzothiadiazole) (hereafter denoted as BBT) is synthesized through palladium-catalyzed Sonogashira-Hagihara cross-coupling polycondensation, and used as a novel organic semiconductor photocatalyst for both photocatalytic H₂ production and pollutant degradation under visible light ($\lambda > 420$ nm) irradiation. Furthermore, BBT/TiO₂ heterojunction is conveniently fabricated through an in-situ polycondensation procedure of 4,7-dibromobenzo[c][1,2,5]thiadiazole and 1,3,5-triethynylbenzene in the presence of commercial TiO₂. After optimizing the composition ratio, the resultant BBT/TiO₂ heterojunction exhibited dramatically enhanced visible-light-responsive photocatalytic activities (~18.0 and 20.4 times higher activity for H₂ evolution and ciprofloxacin degradation, respectively) as compared BBT alone. Detailed investigations revealed that the BBT/TiO₂ heterojunction interface can accelerate the photogenerated electron transferring from BBT to TiO₂, and then improve the photoactivity. The present work exhibits some interesting points and dramatic improvement of photoactivity when an organic semiconductor is combined with an inorganic one, which provides a novel direction to exploit and fabricate photocatalyst for solar energy conversion and pollutant degradation.

© 2016 Elsevier B.V. All rights reserved.

1. Introduction

Nowadays, semiconductor-based photocatalytic technology for solar fuels production and pollutant degradation has been one of the most frontier issues because of the urgent energy and environmental crisis [1–3]. Up till now, most efforts are focused on inorganic semiconductors, such as TiO₂ and other metal oxide/sulfide/nitride [4,5]. However, TiO₂ is limited by its low quantum yield and only UV-light (~4% of solar energy) responsive property due to its wide band-gap (~3.2 eV). In contrast, organic semiconductors are rarely explored in the field of photocatalytic applications for solar fuel production and pollutant degradation. Most recently, as a typical organic semiconductor, g-C₃N₄ has drawn numerous attentions due to its low cost, visible light responsive ability and suitable band edges for water splitting and pollutant

degradation [6,7]. However, the band-gap of g-C₃N₄ is still too wide and cannot absorb visible light longer than ~450 nm, and also the quantum efficiency is still low. Fortunately, the multiformity and tailorability of organic semiconductors may make us explore novel materials with more broad visible-light responsive range and higher quantum efficiency [8,9].

Most recently, conjugated polymers, another emerging organic semiconductors, found their promising applications in visible-light-driven H₂ production and pollutant degradation [10,11]. Different from g-C₃N₄, the semiconductor property and light absorption ability of these conjugated polymers is easily tuned by changing or modifying polymeric monomer. For example, Cooper et al. reported that series of pyrene-based conjugated microporous polymers (CP-CMP1-CP-CMP15) [11] and planarized fluorine-type polymers (P1-P7) [12] could catalyze H₂ production from a sacrificial reagent/water solution under visible light irradiation ($\lambda > 420$ nm) without additional Pt-cocatalyst. Yu et al. also reported porous conjugated polymers (PCPs) based on different chromophore monomers copolymerized with biphenyl/bipyridyl units which are efficient photocatalyst for H₂ production from water/TEA solution in the absence of Pt-cocatalyst [13,14]. Wang et al. designed series of electron-donor-acceptor conjugated poly-

* Corresponding author.

** Corresponding author at: Key laboratory of Environment Correlative Dietology, Ministry of Education, Wuhan 430070, PR China.

E-mail addresses: yxiantg@mail.hzau.edu.cn (Y.-G. Xiang),

hchenhao@mail.hzau.edu.cn (H. Chen).

¹ These authors contributed equally.

benzothiadiazoles for visible-light-driven H₂ production from TEOA/water solution with 3 wt% Pt loading [15]. It should be noted that, all the above mentioned conjugated polymers are synthesized by Suzuki–Miyaura polycondensation with Pd(0)-catalysis. Except for photocatalytic H₂ production, Remita et al. designed one-dimensional poly(diphenylbutadiyne) (PDPB) by photo-polymerization and found it can degrade methyl orange and phenol efficiently under visible light ($\lambda > 450$ nm) irradiation [16]. Also, some other organic semiconductors such as self-assembled PDINH supramolecular are found to be efficient visible-light-responsive photocatalyst for pollutant degradation [17].

Except for exploiting novel visible-light-responsive semiconductors, fabrication of semiconductor-semiconductor composite with matched band edges is an efficient strategy to enhance the photocatalytic ability, as this kind of heterojunction system usually can improve the photogenerated carriers separation efficiency or extend the light responsive region of single semiconductors [5,18–23]. For example, poly(3-hexylthiophene) (P3HT) almost shows no H₂ production activity under visible light even loaded with Pt, but the composite of P3HT with g-C₃N₄ exhibits high photoactivity for H₂ production [19], and P3HT-C₃N₄ have also showed higher photodegradation ability than C₃N₄ [21]. Wan et al. reported that TiO₂-polydopamine would enhance the photodegradation of rhodamine B with high stability [20]. Moreover, polyaniline-CdS composite also benefits visible light induced H₂ production [24].

Since conjugated microporous polymer was firstly reported by Cooper [25], it has been found to possess extensive applications [26,27], such as visible-light-driven organic transformation [28–30], energy device [31,32], gas storage [33]. Based on Sonogashira-Hagihara cross-coupling polycondensation of 4,7-dibromobenzo[c][1,2,5]thiadiazole with 1,3,5-triethynylbenzene, conjugated microporous poly(benzothiadiazole) (CMP_0-CMP_60) were obtained by Vilela et al., which shows photoactivity for conversion of α -terpinene into ascaridole under 420 nm light irradiation [34]. To the best of our knowledge, this type of conjugated microporous polymers based on Sonogashira-Hagihara cross-coupling polycondensation has not been utilized for either photocatalytic H₂ production or pollutant degradation up till now.

Herein, we firstly synthesize pure conjugated microporous poly(benzothiadiazole) according to Vilela's report through Sonogashira-Hagihara cross-coupling polycondensation of 4,7-dibromobenzo[c][1,2,5]thiadiazole with 1,3,5-triethynylbenzene, and the product is named as BBT here. Interestingly, the BBT exhibits subtle photoactivity for H₂ production from water/TEOA solution and degradation of ciprofloxacin under visible light ($\lambda > 420$ nm) irradiation. More importantly, when TiO₂ is added into the polycondensation procedure, a BBT/TiO₂ heterojunction is formed. And the visible-light-driven photoactivity for H₂ production and degradation of ciprofloxacin is improved significantly. The mechanism of the enhanced photocatalytic properties was proposed based on radical detection, photoluminescence spectroscopy (PL), photocurrent, and active species trapping tests and so on. The present paper demonstrates an efficient strategy for improving the photoactivity of conjugated microporous polymers and also a new direction for extending the light responsive region of wide band-gap semiconductors.

2. Experimental section

2.1. Materials

TiO₂ (P25, Degussa), N,N-dimethylformamide (DMF), triethylamine (TEA), triethanolamine (TEOA), methanol, copper(I) iodide (CuI), dichloromethane (DCM) and Pd(PPh₃)₄Cl₂ were obtained

from commercial sources. All of the reagents were analytical reagent and used directly without further purification.

2.2. Synthesis of photocatalyst

Conjugated microporous poly(benzothiadiazole) was synthesized according to the reported procedure [34]. Accordingly, BBT/TiO₂ heterojunction was in-situ obtained as follows. Typically, 300 mg TiO₂ was mixed with DMF/TEA (5 mL/5 mL) solvent, and then dispersed evenly in an ultrasonic bath for 5 min. After that, calculated amount of 1,3,5-triethynylbenzene and 4,7-dibromobenzo[c][1,2,5]thiadiazole with molar ratio of 2:3 along with the catalyst Pd(PPh₃)₄Cl₂ and CuI was added to the above suspension, taking 10.0 wt% BBT/TiO₂ for example, 1,3,5-triethynylbenzene (12.8 mg), 4,7-dibromobenzo[c][1,2,5]thiadiazole (37.5 mg), Pd(PPh₃)₄Cl₂ (3.0 mg) and CuI (1.0 mg) was used. The resulting mixture was stirred at 80 °C under argon for 24 h. The composite was obtained by filtration, continuous washing with DCM and methanol in the Soxhlet for 48 h and finally dried at 60 °C overnight. In this work, seven BBT-TiO₂ composites with weight ratio 1.0 wt%, 3.3 wt%, 6.7 wt%, 10.0 wt%, 13.3 wt%, 16.7 wt% and 20.0 wt% BBT have been synthesized in case of complete conversion of starting materials. The as-prepared BBT/TiO₂ was found to be insoluble in any organic solvent investigated, and the yellow color become deeper and deeper as the ratio of BBT increases gradually.

The fabrication process of BBT/TiO₂/Pt is as same as that of BBT/TiO₂, where the co-catalyst Pt is pre-loaded on TiO₂ by a photoreduction method [35]. Briefly, 0.2 g TiO₂ is dispersed in the mixture of water/methanol solution, and then a calculated amount of H₂PtCl₆ solution is added, after which the mixture is irradiated by a 36 W UV lamp for 3 h. And then, the suspension is centrifuged and dried under 60 °C to afford the Pt/TiO₂ catalyst.

2.3. Characterization

X-ray diffraction (XRD) patterns of the samples were obtained on a X-ray diffractometer (D8 advance Bruker Inc., Germany) with Cu K α radiation source at 40 kV. Solid state NMR experiments were carried out to check chemical structure of BBT and BBT-TiO₂, using Bruker Avance 400 MHz spectrometer equipped with standard 4 mm magic angle spinning (MAS) double resonance probe head. The scanning electron microscopy (SEM) was operated on JSM-6700F JEOL. Thermogravimetric Analysis (TGA) was conducted using a NETZSCH TG209 instrument with a heating rate at 10 °C/min under air atmosphere. The specific Brunauer–Emmett–Teller (BET) surface area of BBT, TiO₂ and BBT/TiO₂ were obtained by nitrogen adsorption-desorption isotherms methods using Micrometrics ASAP 2040. Raman spectra were investigated on a microscopic confocal Renishaw 1000 NR Raman spectrometer. UV-vis diffuse reflectance spectra (DRS) were recorded in the range from 200 nm to 700 nm using Shimadzu UV-3100. X-ray photoelectron spectrometer (XPS) was performed on XSAM800 system. The steady-state photoluminescence (PL) measurements of BBT, BBT/TiO₂ were investigated with Hitachi F-4600 excited at 450 nm. The cyclic voltammetry (CV) measurement were conducted on a CHI 660E workstation using a standard three-electrode cell with glassy carbon electrode as the working electrode, Ag/Ag⁺ electrode as the reference electrode, platinum plate as the counter electrode, and 0.1 M TBAPF₆ solution in acetonitrile was used as supporting electrolyte. The potential was recorded against the ferrocene/ferrocenium (Fc/Fc⁺). For the conversion from Fc/Fc⁺ redox couple to the Normal Hydrogen Electrode (NHE), the equation E_{NHE} = E_{Fc/Fc⁺} + 0.63 V was applied. Superoxide radical anions (•O₂[−]) and hydroxyl radicals (•OH) of BBT/TiO₂ were detected utilizing

Electron spin resonance (ESR) spectra employing 5,5-dimethyl-1-pyrroline-N-oxide (DMPO) as the electron spin trapper.

2.4. Measurement of photocatalytic activity

The photocatalytic activity of BBT/TiO₂ composites, pure TiO₂ and BBT was evaluated by photocatalytic H₂ production, photodegradation of ciprofloxacin and phenol under visible light irradiation, and a 300 W Xe lamp (PLS SXE300, Beijing Perfectlight Inc., China) equipped with a 420 nm cut-off filter is used as light source.

The H₂ production test is carried out in a typical photocatalytic system as our previous report [36]. Typically, 30 mg BBT/TiO₂/Pt is dispersed in 30 mL 10% vol TEOA/water, and irradiated under $\lambda > 420$ nm by a 300 W Xe-lamp with a cutoff filter ($\lambda > 420$ nm) or band-pass filters ($\lambda = 420, 500$ nm etc.) after thoroughly removing air. For the photocatalytic conditions optimization, 10 mg catalyst suspended in 10 mL TEOA/water was adopted. The H₂ production rate is tested by a GC (SP7820, TCD detector, 5 Å molecular sieve columns, and Ar carrier).

The apparent quantum yield (AQY) for photocatalytic H₂ production is calculated as follows [37,38]:

$$\text{AQY (\%)} = \frac{2 \times \text{Number of evolved H}_2 \text{ molecules}}{\text{Number of incident photons}} \times 100\% = \frac{2 \times C \times N_A}{S \times P \times t \times \lambda / (h \times c)} \times 100\%$$

Where, C is the H₂ production amount (μmol) per hour; N_A is Avogadro constant ($6.02 \times 10^{23}/\text{mol}$); P is incident monochromatic light intensity (W/cm^2); S is the irradiation area (19.6 cm^2 , a cylindrical photoreactor with diameter of 5 cm); t is the light irradiation time (1 h); λ is the monochromatic light wavelength (nm); h is Plank constant ($6.626 \times 10^{-34} \text{ Js}$); c is vacuum light velocity ($3 \times 10^8 \text{ m/s}$); the monochromatic light intensity (detected by a calibrated Si photodiode (SRC-1000-TC-QZ-N, Oriel, USA)) of 420, 450, 500, 520, 600, 650 and 700 nm is 22.8, 37.0, 47.0, 46.1, 53.4, 63.1 and 36.6 mW/cm² respectively.

For ciprofloxacin and phenol photodegradation, 10 mg of the photocatalyst was dispersed in an aqueous solution of ciprofloxacin (CIP, 50 mL, 20 ppm) or phenol (50 mL, 20 ppm). Before irradiation, the suspension was stirred in dark for 60 min to reach adsorption-desorption equilibrium. During the illumination, about 4 mL aliquot was sampled at the interval 5 min over 20 min (CIP) or 20 min over 120 min (phenol), and the solid was removed by filtration. The concentration of CIP and phenol was analyzed by recording the signal intensity using HPLC method with a UV detector at 275 nm and 270 nm, respectively. After the degradation experiment was completed, the catalyst was recycled by centrifuge, washed with methanol thoroughly, and dried at 60 °C overnight. The collected catalyst was used for the next cycle of CIP degradation in the same condition.

2.5. Photocurrent and EIS tests

Photocurrent and EIS behaviors are carried out on a CHI 660E electrochemical analyzer equipped with a three-electrode cell. The working electrode is made as follows: certain amount of catalyst is mixed with 5 wt% Nafion, and then fixed on a FTO conducting glass by a doctor-blade technique. Pt plate and Ag/AgCl are used as the counter and reference electrode, respectively, and 0.1 M Na₂SO₄ as electrolyte. A 300 W Xe-lamp with a 420 nm cur-off filter served as the light source.

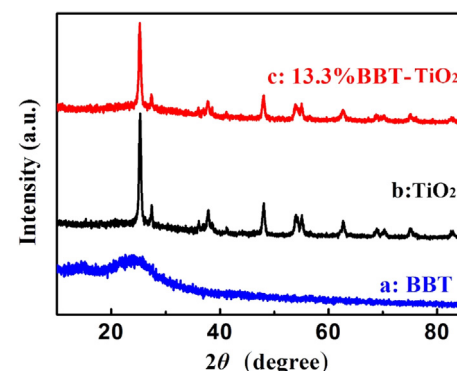


Fig. 1. XRD patterns of BBT, 13.3% BBT-TiO₂ and TiO₂.

3. Results and discussion

3.1. BBT/TiO₂ composite structure and composition analyses

Fig. 1 displays the XRD patterns of the obtained BBT, 13.3% BBT/TiO₂ composite and TiO₂. As can be seen, TiO₂ exhibits a mixed phase of tetragonal anatase TiO₂ (JCPDS 21-1272) with characteristic diffraction peaks at $2\theta = 25.3^\circ, 37.9^\circ, 48.1^\circ, 54.1^\circ, 55.2^\circ, 62.8^\circ$ and tetragonal rutile TiO₂ (JCPDS 21-1276) with characteristic diffraction peaks at $2\theta = 27.4^\circ, 36.1^\circ$. No obvious diffraction peaks can be found in BBT, indicating the amorphous phase of BBT. Simultaneously, 13.3% BBT/TiO₂ exhibits the same XRD pattern as that of TiO₂, indicating that the polymerization procedure has no influence on TiO₂, and no XRD patterns attributing to BBT are observed probably due to the low loading amount and high dispersion of BBT on TiO₂. This point can be confirmed by the following TEM picture. Thermo-gravimetric measurements were conducted to get the exact content of BBT in the composite 13.3% BBT/TiO₂, and it revealed that ratio of BBT is about 12.4% which is approximated to the calculated ratio (Fig. S1).

Various element species in BBT/TiO₂ composite can be determined by XPS spectra shown in Fig. S2a. The survey spectrum reveals that Ti, S, C, N, O exist in the 13.3% BBT/TiO₂. Table S1 shows the binding energy of Ti2p, S2p, C1s, N1s, O1s peaks for BBT, TiO₂ or BBT/TiO₂. As can be seen, both TiO₂ and the composite show the binding energy at 458.4 and 464.2 eV representing Ti 2p_{3/2} and Ti 2p_{1/2} without obvious shift (Fig. S2b). The spectrum of S 2p can be deconvoluted into three peaks at 165.6, 166.9 and 170.6 eV, and the first two peaks represent the neutral sulfur with the third one assigning to oxidized species, and no binding energy changes for all these three peaks (Fig. S2c). However, the binding energy at 399.5 and 399.9 eV for N 1s in BBT shows blue-shift to 399.3 and 399.7 eV for N 1s in the composite (Fig. 2a), respectively. Meanwhile, XPS peaks of O 1s can be deconvoluted into two characteristic peaks at 529.9 and 531.7 eV in TiO₂ which are assigned to Ti–O bond and surface hydroxyl group, respectively. However, the corresponding peaks appear at 529.9 and 532.1 eV (Fig. 2b), and an obvious red-shift is observed. The blue-shift of N1s binding energy and red-shift of O1s binding energy implying that there may exists strong interaction between BBT and TiO₂ [21,39], which will facilitate the charge transfer between BBT and TiO₂ under visible light irradiation.

The tight interaction between BBT and TiO₂ of BBT/TiO₂ can be further supported by Raman spectra. As shown in Fig. 3, TiO₂ exhibits characteristic peaks at 146 cm^{-1} ($E_{g(1)}$) 401 cm^{-1} (B_{1g}), 520 cm^{-1} (A_{1g}) and 642 cm^{-1} ($E_{g(2)}$). Weak peaks of BBT appeared at 1364 cm^{-1} , 1537 cm^{-1} and 2204 cm^{-1} which are attributed to the C=C backbone stretching, ring stretching and C≡C backbone stretching of BBT. The BBT/TiO₂ exhibits both peaks of TiO₂ and

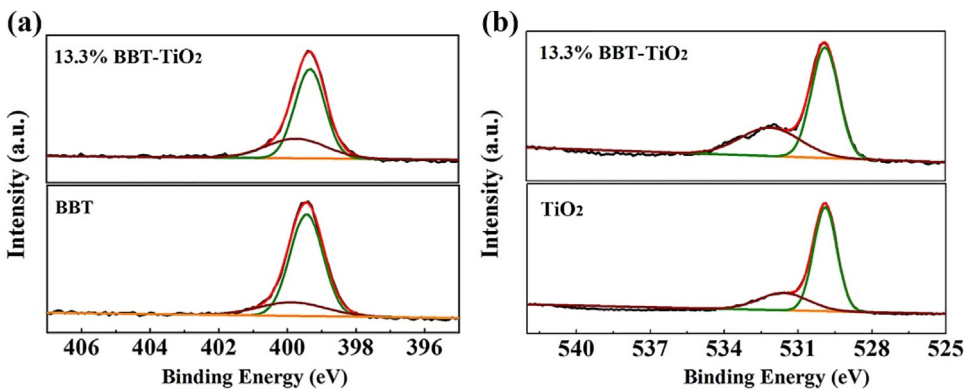


Fig. 2. XPS spectra of BBT, TiO₂, 13.3% BBT/TiO₂. (a) N 1s. (b) O 1s.

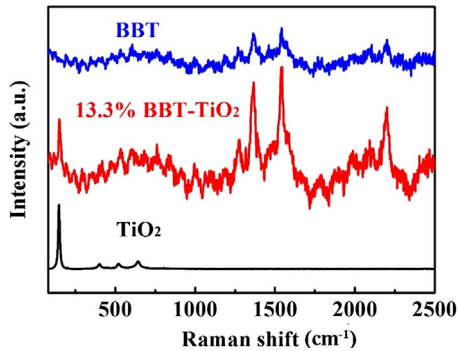


Fig. 3. Raman spectra of BBT, 13.3% and TiO₂.

BBT, and the decreasing of TiO₂ peaks should be caused by the coating of BBT on its surface. In comparison with BBT, the Raman peaks intensity of BBT in the composite increased greatly due to the pre-resonance effect, indicating that more ordered and longer conjugated segments formed in the BBT/TiO₂ composites.

Solid state ¹³C NMR spectra were then employed to confirm the chemical structure of pure BBT and BBT in the composite. As shown

in Fig. 4, pure BBT exhibited broad peaks with 153.9, 132.8, 123.6, 116.8 ppm assigning to aromatic carbons, and peaks at 95.9 and 87.6 ppm attributing to C≡C groups, which are consistent with the reported data [34]. While BBT are in-situ generated in the presence of TiO₂, the composite display similar NMR spectra, and it clearly indicated that BBT could also formed in the same condition.

Fig. 5 depicts the DRS spectra of TiO₂, BBT and 13.3% BBT/TiO₂. As can be seen, TiO₂ exhibits no any visible light absorption ability due to its wide band-gap, while BBT shows a broad absorption in visible light range up to ~700 nm. More importantly, 13.3% BBT/TiO₂ shows strong visible light absorption ability from 400 nm to ~700 nm, which combine the characteristic absorption region of both BBT and TiO₂ [19,21], indicating the BBT/TiO₂ can be excited by visible light for photocatalytic applications.

3.2. Photocatalytic H₂ production ability of BBT/TiO₂ composite

To evaluate the photocatalytic ability of BBT/TiO₂ composites, the catalyst was found to work when utilized for photocatalytic H₂ production with Pt as co-catalyst and TEOA as sacrificial reagent under visible light ($\lambda > 420$ nm) irradiation. As shown in Fig. 6, Pt/TiO₂ gives no any H₂ production activity, indicat-

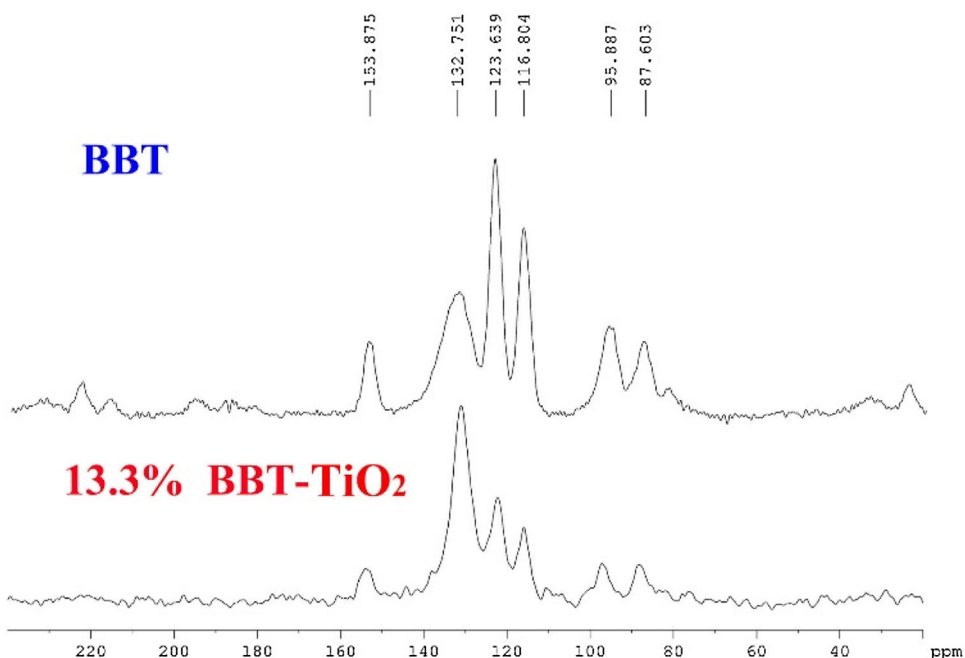


Fig. 4. Solid-state ¹³C-CP/MAS NMR of BBT and BBT-TiO₂.

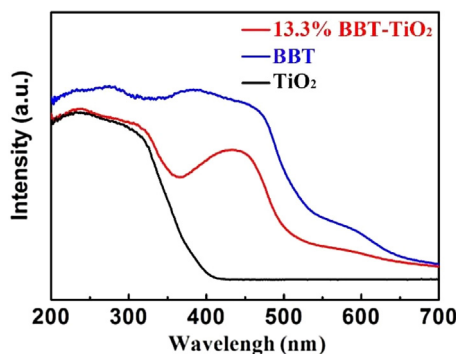


Fig. 5. UV/Vis diffuse reflectance spectra of BBT, TiO₂ and 13.3% BBT-TiO₂.

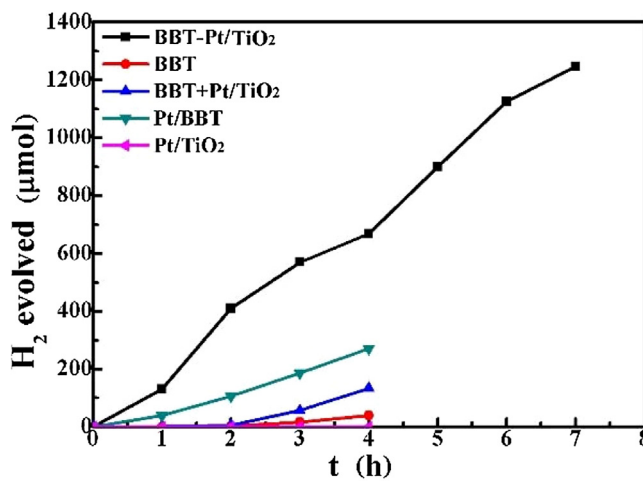


Fig. 6. Compared photocatalytic H₂ production activity of BBT, Pt/TiO₂ and BBT-Pt/TiO₂ under visible light irradiation. Conditions: 30 mg BBT-Pt/TiO₂, 0.5 wt% Pt, 6.7 wt% BBT, 30 mL 10% vol TEOA/H₂O, $\lambda > 420$ nm. Notes: Pt/BBT is in-situ formed by adding H₂PtCl₆ (corresponding to 0.5 wt% loading amount) aqueous solution to BBT and TEOA/H₂O suspension before irradiation; simple mixture of BBT and Pt/TiO₂ is formed by grinding them together uniformly.

ing the band-gap excitation of TiO₂ is impossible in the present conditions. BBT shows low photocatalytic H₂ production activity ($\sim 330 \mu\text{mol}/\text{h/g}$) though it possess excellent visible light absorption ability as shown in DRS spectrum. However, the 6.7 wt% BBT/TiO₂/Pt exhibits robust H₂ production ability in the tested 7 h and up to $\sim 1246 \mu\text{mol}$ H₂ is detected, which corresponds to a H₂ production rate of $\sim 5933 \mu\text{mol}/\text{h/g}$, ~ 18.0 times higher than that of pure BBT. For comparison, a simple mixture of BBT and Pt/TiO₂ (that is BBT+Pt/TiO₂) and Pt/BBT are also tested for photocatalytic H₂ production under visible light irradiation. As can be seen, the two samples shows much lower photoactivity than that of in-situ formed BBT/TiO₂. These results indicate that the composite of BBT and Pt/TiO₂ as well as the tight interaction between BBT and Pt/TiO₂ are important to enhance the photogenerated carriers separation and then for photocatalytic H₂ production. And the existence of tight interaction can be clearly supported by the above XPS and Raman analysis and the following TEM section.

Fig. 7 gives the effect of BBT and Pt loading amount on the H₂ production activity over BBT/TiO₂/Pt. No obvious H₂ production is detected when no BBT is loaded on Pt/TiO₂, however, significant amount of H₂ is detected even 1.0 wt% BBT is loaded under visible light irradiation, indicating the H₂ production activity is originated by the visible light absorption ability of BBT, as can be seen from the DRS spectra in Fig. 5. The H₂ production activity is enhanced with increasing amount of BBT, which reaches to the highest value of $\sim 6750 \mu\text{mol}/\text{h/g}$ with 6.7 wt% loading amount of BBT. In addi-

tion, the H₂ production activity decreases with further increasing BBT loaded amount (Fig. 7a), and this phenomenon could also been observed in the process of photocatalytic degradation of CIP (see following section), as excessive more BBT loading affects the photoelectron injection from BBT to TiO₂ and the reaction between H⁺ and e⁻ on Pt cocatalyst. Pt, as cocatalyst, is always necessary for most H₂ production photocatalyst [40]. As shown in Fig. 7b, Pt also can significantly affect the H₂ production activity of BBT/TiO₂/Pt, and the H₂ production activity exhibits a typical inverted parabola curve with increasing Pt loading amount. Generally, Pt cocatalyst can act as H₂ production sites, debasing hydrogen evolution over potential and promote charge carriers separation. Therefore, the H₂ production rate will first increase with loading of Pt on catalyst, however, excessive Pt loading will be harmful because it may cover some active sites on catalyst and increase charge recombination [40]. Further deep investigation of photocatalytic H₂ production property of the similar polymers is in progress by our group now.

3.3. Photocatalytic degradation ability of BBT/TiO₂ composite

In addition to the excellent property of BBT/TiO₂ in H₂ production, the as-prepared catalyst has also been applied to pollutant degradation. Fig. 8 compares the photoactivity of TiO₂, BBT and BBT/TiO₂ for degradation ciprofloxacin and phenol in aqueous solution under $\lambda \geq 420$ nm. Blank experiment exhibits that the self-photodegradation of CIP under visible light can be neglected. As shown in Fig. 8a, TiO₂ shows no obvious photoactivity because it cannot be excited by visible light, and only 9% of 20 ppm CIP can be degraded by BBT in the same condition though it possess broad and strong visible light absorption ability. However, the BBT/TiO₂ composites exhibit much better photodegradation performance than that of BBT. As the content of BBT increase from 6.7% to 13.3%, the photocatalytic ability are promoted gradually, however, the degradation rate is reduced if the content of BBT continues to increase. Accordingly, 13.3% BBT/TiO₂ shows the highest photocatalytic ability in terms of CIP degradation, and it is inferred that aggregation of more BBT than the threshold ratio between BBT and TiO₂ will hinder the separation efficiency of photogenerated electrons and holes [41]. It reveals that all the degradation progresses follow first-order dynamic models (Fig. S3a), and the kinetic rate constant of 13.3% BBT/TiO₂ is 20.4 times of that of BBT (Fig. 8b). Moreover, the mechanical mixture of 13.3% BBT/TiO₂ is also applied in the photodegradation of CIP, which could only show similar photocatalytic ability to pure BBT. The 13.3% BBT/TiO₂ also show significant high photocatalytic activity of phenol (Fig. 8c) in the way of first-order dynamic models (Fig. S3b). Recycling experiments have been carried out to evaluate the stability of BBT-TiO₂ composites, and the photoactivity of 13.3% BBT/TiO₂ catalyst shows no obvious decrease after 3 runs (Fig. 8d).

In general, photocatalytic oxidation involves in diverse active species, and ESR experiments here is conducted to confirm whether photogenerated superoxide radical anion (•O₂⁻) and hydroxyl radical (•OH) exist in 13.3% BBT/TiO₂ under visible light or not. It is well known that •O₂⁻ and •OH are produced once molecule O₂ are reduced by single electron and molecules H₂O molecule are oxidized by hole, and spin adducts DMPO-•O₂⁻ and DMPO-•OH form while photogenerated •O₂⁻ and •OH are trapped by DMPO. As shown in Fig. 9a, strong characteristic signals of DMPO-•O₂⁻ and DMPO-•OH spin adducts could be found in the suspension of 13.3% BBT/TiO₂ composite, indicating •O₂⁻ and •OH radicals may participate in photodegradation of CIP. As the LUMO of BBT (1.44 eV) is not positive enough to oxidize the water or surface hydroxyl group (2.38 eV vs. NHE) to generate •OH, the strong signals of DMPO-•OH may arise from further conversion of •O₂⁻ [42].

Apart from ESR measurement, it is also of great significance to further find out the active species that dominate the CIP

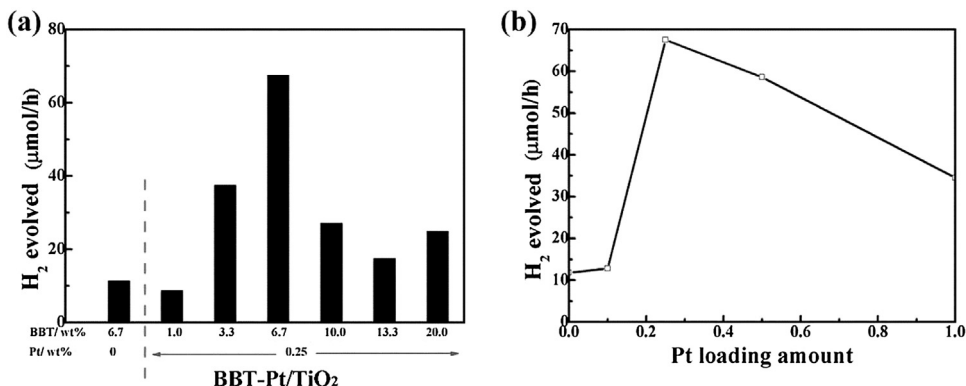


Fig. 7. Effect of (a) BBT and (b) Pt loading amount on the H₂ production activity over BBT-Pt/TiO₂. Conditions: 10 mg BBT-Pt/TiO₂, 10 mL 10% vol TEOA/H₂O, $\lambda > 420$ nm.

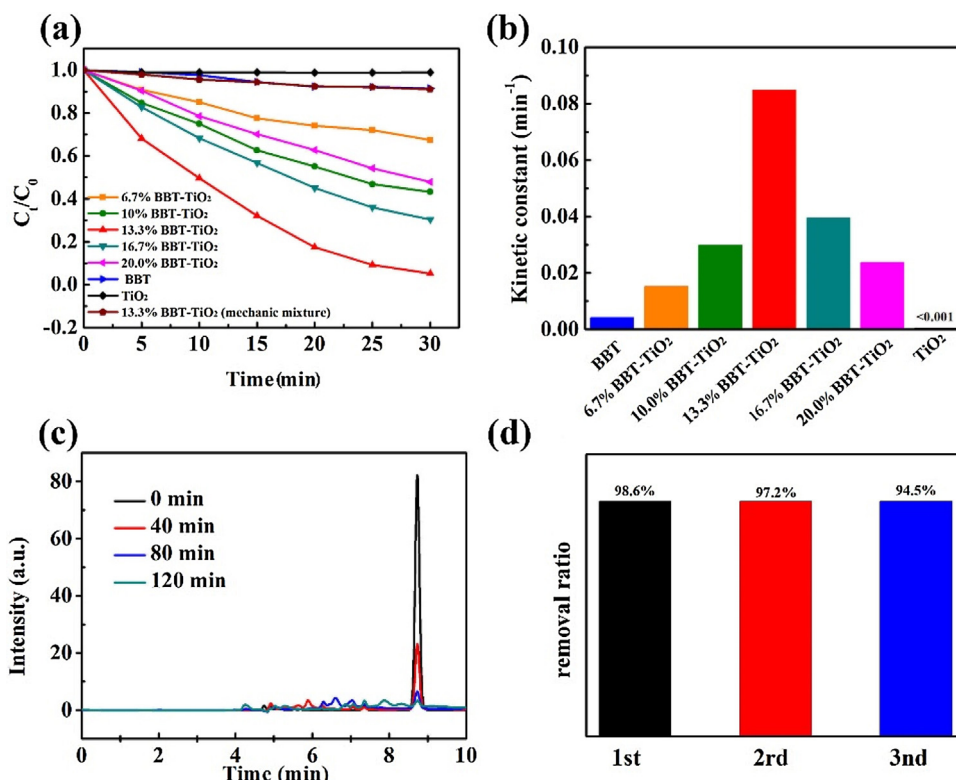


Fig. 8. (a) Photodegradation of ciprofloxacin with visible light irradiation in the presence of BBT, pure TiO₂, BBT-TiO₂ composites. Photocatalytic degradation efficiencies between C_t/C₀ and irradiation time. (b) Reaction rate constant comparison among different samples. (c) The degradation rate of phenol. (d) Cycling measurement in photocatalytic degradation of ciprofloxacin with 13.3% BBT-TiO₂ composite as the photocatalyst.

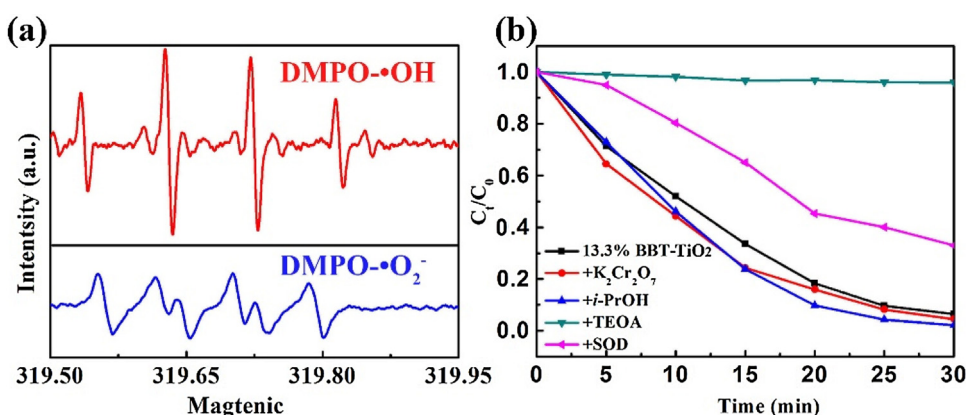


Fig. 9. (a) ESR spectra of DMPO-•OH and DMPO-•O₂⁻ for 13.3% BBT-TiO₂. (b) Trapping measurement with different scavenger (IPA → •OH, K₂Cr₂O₇ → e⁻, SOD → •O₂⁻, TEOA → h⁺) for photodegradation of CIP.

photodegradation process, and trapping experiments were performed using isopropanol, $K_2Cr_2O_7$, superoxide dismutase (SOD) and triethanolamine (TEOA) to scavenger hydroxyl radicals ($\cdot OH$), electron (e^-), superoxide radical anions ($\cdot O_2^-$) and hole (h^+), respectively (Fig. 9b). The results indicated that addition of isopropanol and $K_2Cr_2O_7$ did not change the photodegradation rate significantly, however, about 67% of CIP has been degraded in the presence of SOD while only 4.2% of 20 ppm CIP could be consumed using TEOA as scavenger over 30 min. Accordingly, holes and $\cdot O_2^-$ are the main active species participating in the photodegradation of CIP, and it further proved that BBT/TiO₂ composites benefit generation of holes and $\cdot O_2^-$ under visible light.

3.4. Photocatalytic mechanism discussion on BBT/TiO₂

The visible-light-responsive photocatalytic ability can be caused by the BBT in the BBT/TiO₂ heterojunction, which can be confirmed by the DRS spectrum and the fact that BBT and BBT/TiO₂ but not TiO₂ show photocatalytic activity for both photodegradation and photocatalytic H₂ production. Fig. 10 depicts the photocatalytic H₂ production activity and corresponding AQY values of BBT/TiO₂/Pt under series of monochromatic light irradiation. As can be seen, the tendency of H₂ production rate and AQY along with the irradiation light seems as same as that of the DRS spectra of BBT/TiO₂, indicating that the BBT on TiO₂ governs the whole visible-light-driven photocatalytic H₂ production. Especially, the highest AQY of 1.45% is obtained at $\lambda = 450$ nm, which is in accordance with the maximal absorption peak of BBT. Similarly, taken the photodegradation

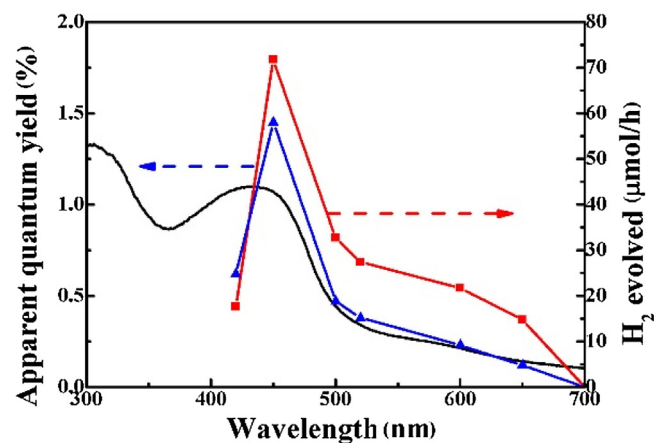


Fig. 10. Comparison of DRS and wavelength dependent photocatalytic H₂ production of BBT-Pt/TiO₂. Conditions: 30 mg BBT-Pt/TiO₂, 0.5 wt% Pt, 6.6 wt% BBT, 30 mL 10% vol TEOA/H₂O, $\lambda = 420, 450, 500, 520, 600, 650$ and 700 nm.

activity in Fig. 8b as example, only 13.3% BBT in BBT/TiO₂ Exhibits 20.4 times higher photoactivity than that of the pure BBT. The significant enhancement of photoactivity for BBT after composition with TiO₂ should be rationalized as follows.

- (1) The morphology of BBT is changed absolutely and an intimate heterojunction structure is formed as shown in Fig. 11. The pure

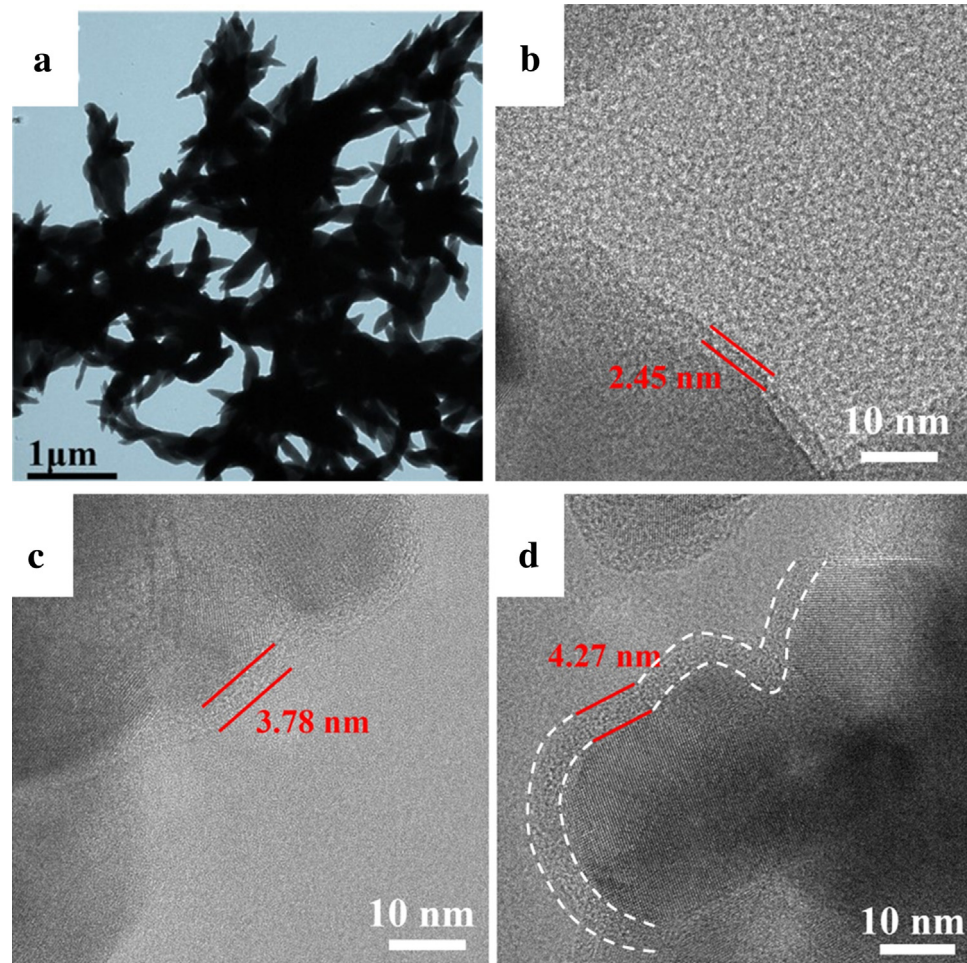


Fig. 11. TEM images of (a) BBT, (b) 6.7% BBT-TiO₂, (c) 13.3% BBT-TiO₂, (d) 20.0% BBT-TiO₂.

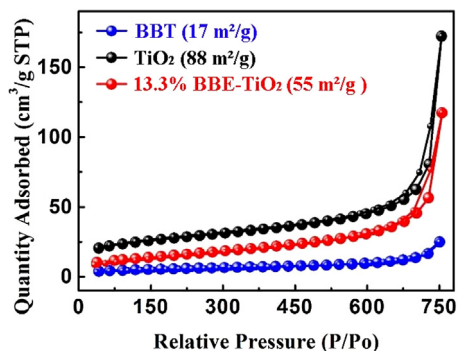


Fig. 12. N_2 -adsorption-desorption isotherms of BBT, TiO_2 and 13.3% BBT-TiO₂.

BBT only exhibits a rod-like structure, while the BBT covers the TiO_2 surface to form a heterojunction structure when the BBT is in-situ polycondensed on TiO_2 particles, and there are tight contact between the crystallized TiO_2 and amorphous BBT (no obvious lattice fringe is observed), indicating the formation of heterojunction. Simultaneously, as amount ratio of BBT in the composites increase from 6.7% to 20.0%, the thickness of BBT gradually grows from 2.45 nm to 4.27 nm. That is, the morphology of BBT, the dispersion of BBT on TiO_2 and the interaction between BBT and TiO_2 can be significantly changed during the present in-situ polycondensation procedure in the presence of TiO_2 . As we know, the morphology and intrinsic interaction of a composite catalyst can greatly affect its photocatalytic performance.

(2) The BET surface areas of BBT/TiO₂ increase significantly compared to that of BBT. As indicated in Fig. 12, the surface areas of BBT, TiO_2 and 13.3% BBT/TiO₂ were 17, 88 and 51 m^2/g , respec-

tively. That is, the surface areas of 13.3% BBT/TiO₂ is 3 times than that of BBT. As we know, either H₂ production or photodegradation involves interface reaction and surface adsorption of reaction substrate in a suspension of catalyst, which will be significantly affected by the surface areas of catalyst.

- (3) The photogenerated charge separation efficiency is much higher in BBT/TiO₂ than that of BBT. Fig. 13a reveals that the photocurrents of BBT/TiO₂ is much higher than that of BBT under visible light, indicating that the photogenerated charge separation efficiency of BBT/TiO₂ can be significantly improved once BBT is excited by visible light (TiO_2 cannot be excited by visible light and shows almost no any photocurrent signal). It reveals that the formed heterojunction between BBT and TiO_2 can accelerate the e⁻/h⁺ separation and then benefit for the enhancement of photocatalytic activities for either H₂ production or pollutant degradation. Moreover, BBT/TiO₂ heterojunction shows smaller arc radius in the EIS Nyquist plot than that of TiO_2 , revealing that more efficient separation of photogenerated charge occurred (Fig. S4). Furthermore, the PL spectra also indicate an efficient photogenerated electron transfer from BBT to TiO_2 since the emission peak (at $\lambda_{\text{em}} \sim 530 \text{ nm}$) of BBT decreases significantly in the case of BBT/TiO₂ composite excited by $\lambda_{\text{ex}} = 450 \text{ nm}$ as can be seen from Fig. 13b.
- (4) The above-mentioned electron transfer between BBT and TiO_2 should be confirmed thermodynamically. The HOMO-LUMO bandgap of BBT is determined to be 2.12 eV according to the absorption edge of DRS spectra, and the LUMO potential of BBT was -0.68 eV vs. NHE measured by cyclic voltammetry method (see Fig. S5), and HOMO potential of BBT was calculated at 1.44 eV according to HOMO potential and band gap. It is well

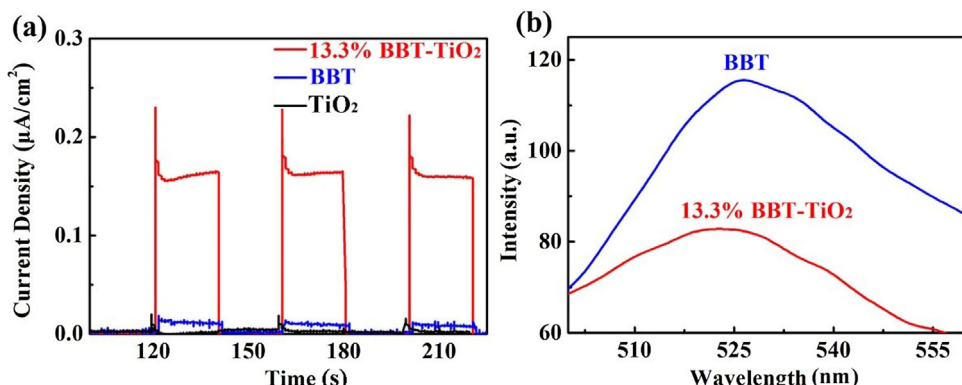


Fig. 13. (a) The photocurrent generated by TiO_2 , BBT and 13.3% BBT-TiO₂ under visible light. (b) PL spectra of BBT and 13.3% BBT-TiO₂ excited at 450 nm.

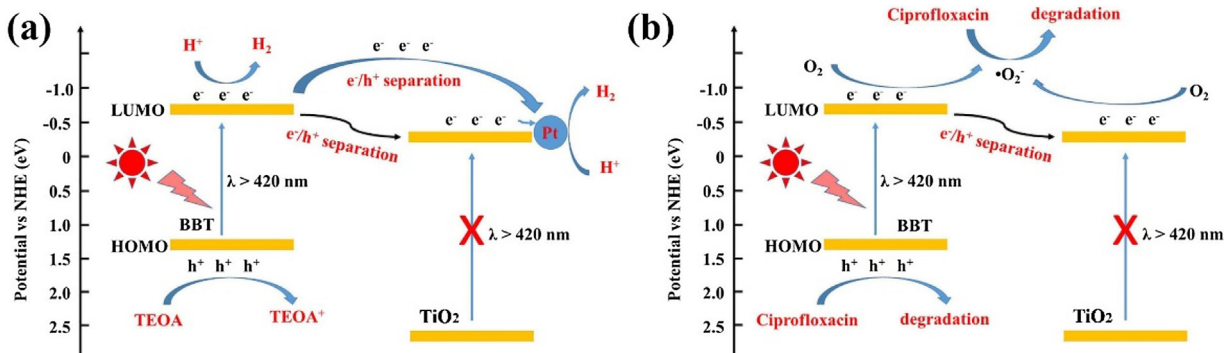


Fig. 14. Proposed mechanism for (a) photocatalytic H₂ production and (b) photodegradation of CIP over BBT-TiO₂ heterojunction.

known that the CB level of TiO₂ is -0.5 eV , and the electron transfer from LUMO of BBT to the CB of TiO₂ is favorable [22].

Based on the above results and discussions, a possible mechanism for the photocatalytic H₂ production and CIP photodegradation of the present BBT/TiO₂ heterojunction is proposed as shown in Fig. 14a. Since only BBT can be excited by visible light in the composite of BBT/TiO₂, and the photogenerated electron jumped from HOMO into the LUMO of BBT, and then injected into the CB band of TiO₂. Except for the promoting effect of e⁻/h⁺ separation by TiO₂, the loading of cocatalyst Pt can further accelerate the electron transfer. Finally, the electron in LUMO of BBT and Pt sites can participate in H₂ production. Similarly, those electrons injected into CB of TiO₂ as well as some electrons in LUMO of BBT can react with O₂ to form •O₂⁻, which will participate in the CIP photodegradation together with h⁺ in HOMO of BBT (Fig. 14b). It must be noted that the formation of heterojunction structure is a key role to enhance the photogenerated charge separation, which then causing the enhanced photoactivity for either H₂ production or pollutant degradation.

4. Conclusions

In summary, a high efficient BBT/TiO₂ heterojunction photocatalyst is fabricated by in-situ polymerization of conjugated microporous poly(benzothiadiazole) and TiO₂. Under optimal conditions, the photoactivities of BBT/TiO₂ are ~ 18.0 and ~ 20.4 times higher than that of pure BBT for photocatalytic H₂ production and photodegradation of CIP under $\lambda > 420\text{ nm}$ respectively. According to systemic investigation, it is found that the formation of heterojunction, the efficient electron transfer from BBT to TiO₂ for improving e⁻/h⁺ separation are the key roles for the significant enhancement of photoactivities. Moreover, strategies of in-situ fabrication of CMP-semiconductors are expected to be applied in the field of photocatalytic CO₂ reduction, organic solar cells and so on.

Acknowledgements

The research was financially supported by the National Natural Science Foundation of China (51572101, 21502059 and 21607047), and the Fundamental Research Funds for the Central Universities (2662014BQ061, 2662015QD019, 2016PY088, 2015PY120 and 2015PY047).

Appendix A. Supplementary data

Supplementary data associated with this article can be found, in the online version, at <http://dx.doi.org/10.1016/j.apcatb.2016.10.059>.

References

- [1] J. Willkomm, K.L. Orchard, A. Reynal, E. Pastor, J.R. Durrant, E. Reisner, Chem. Soc. Rev. 45 (2016) 9–23.
- [2] S.W. Cao, J.X. Low, J.G. Yu, M. Jaroniec, Adv. Mater. 27 (2015) 2150–2176.
- [3] S.Y. Wang, C.W. Liu, K. Dai, P. Cai, H. Chen, C.J. Yang, Q.Y. Huang, J. Mater. Chem. A 3 (2015) 21090–21098.
- [4] X.B. Chen, L. Liu, F.Q. Huang, Chem. Soc. Rev. 44 (2015) 1861–1885.
- [5] Y. Ma, X.L. Wang, Y.S. Jia, X.B. Chen, H.X. Han, C. Li, Chem. Rev. 114 (2014) 9987–10043.
- [6] X.C. Wang, K. Maeda, A. Thomas, K. Takanabe, G. Xin, J.M. Carlsson, K. Domen, M. Antonietti, Nat. Mater. 8 (2009) 76–80.
- [7] Y. Zheng, L.H. Lin, B. Wang, X.C. Wang, Angew. Chem. Int. Ed. 54 (2015) 12868–12884.
- [8] H.F. Yao, L. Ye, H. Zhang, S.S. Li, S.Q. Zhang, J.H. Hou, Chem. Rev. 116 (2016) 7397–7457.
- [9] L.Y. Lu, T.Y. Zheng, Q.H. Wu, A.M. Schneider, D.L. Zhao, L.P. Yu, Chem. Rev. 115 (2015) 12666–12731.
- [10] V.S. Vyas, B.V. Lotsch, Nature 521 (2015) 41–42.
- [11] R.S. Sprick, J.X. Jiang, B. Bonillo, S.J. Ren, T. Ratvijitvech, P. Guiglion, M.A. Zwijnenburg, D.J. Adams, A.I. Cooper, J. Am. Chem. Soc. 137 (2015) 3265–3270.
- [12] R.S. Sprick, B. Bonillo, R. Clowes, P. Guiglion, N.J. Brownbill, B.J. Slater, F. Blanc, M.A. Zwijnenburg, D.J. Adams, A.I. Cooper, Angew. Chem. Int. Ed. 55 (2016) 1792–1796.
- [13] L.W. Li, Z.X. Cai, Q.H. Wu, W.Y. Lo, N. Zhang, L.X. Chen, L.P. Yu, J. Am. Chem. Soc. 138 (2016) 7681–7686.
- [14] L.W. Li, R.G. Hadt, S.Y. Yao, W.Y. Lo, Z.X. Cai, Q.H. Wu, B. Pandit, L.X. Chen, L.P. Yu, Chem. Mater. 28 (2016) 5394–5399.
- [15] C. Yang, B.C. Ma, L.Z. Zhang, S. Lin, S. Ghasimi, K. Landfester, K.A.I. Zhang, X.C. Wang, Angew. Chem. Int. Ed. 55 (2016) 9202–9206.
- [16] S. Ghosh, N.A. Kouame, Laurence Ramos, S. Remita, A. Dazzi, A. Deniset-Besseau, P. Beaunier, F. Goubard, P.-H. Aubert, H. Remita, Nat. Mater. 14 (2016) 505–511.
- [17] D. Liu, J. Wang, X.J. Bai, R.L. Zong, Y.F. Zhu, Adv. Mater. 28 (2016) 7284–7290.
- [18] K. Li, B. Chai, T.Y. Peng, J. Mao, L. Zan, ACS Catal. 3 (2013) 170–177.
- [19] H.J. Yan, Y. Huang, Chem. Commun. 47 (2011) 4168–4170.
- [20] W.X. Mao, X.J. Lin, W. Zhang, Z.X. Chi, R.W. Lyu, A.M. Cao, L.J. Wan, Chem. Commun. 52 (2016) 7122–7125.
- [21] X.J. Bai, C.P. Sun, S.L. Wu, Y.F. Zhu, J. Mater. Chem. A 3 (2015) 2741–2747.
- [22] B. Chai, T.Y. Peng, J. Mao, K. Li, L. Zan, Phys. Chem. Chem. Phys. 14 (2012) 16745–16752.
- [23] B. Chai, T.Y. Peng, P. Zeng, J. Mao, J. Mater. Chem. 21 (2011) 14587–14593.
- [24] K. He, M.T. Li, L.J. Guo, Int. J. Hydrogen Energy 37 (2012) 755–759.
- [25] J.X. Jiang, F. Su, A. Trewin, C.D. Wood, N.L. Campbell, H. Niu, C. Dickinson, A.Y. Ganin, M.J. Rosseinsky, Y.Z. Khimyak, A.I. Cooper, Angew. Chem. Int. Ed. 46 (2007) 8574–8578.
- [26] Y.H. Xu, S.B. Jin, H. Xu, A. Nagai, D.L. Jiang, Chem. Soc. Rev. 42 (2013) 8012–8031.
- [27] A.G. Slater, A.I. Cooper, Science 348 (2015) aaa8075.
- [28] R. Li, Z.J. Wang, L. Wang, B.C. Ma, S. Ghasimi, H. Lu, K. Landfester, K.A.I. Zhang, ACS Catal. 6 (2016) 1113–1121.
- [29] X. Wang, S.M. Lu, J. Li, Y. Liu, C. Li, Catal. Sci. Technol. 5 (2015) 2585–2589.
- [30] Z.J. Wang, S. Ghasimi, K. Landfester, K.A.I. Zhang, Chem. Mater. 27 (2015) 1921–1924.
- [31] F. Xu, X. Chen, Z.W. Tang, D.C. Wu, R.W. Fu, D.L. Jiang, Chem. Commun. 50 (2014) 4788–4790.
- [32] X.D. Zhuang, D. Gehrig, N. Forler, H.W. Liang, M. Wagner, M.R. Hansen, F. Laquai, F. Zhang, X.L. Feng, Adv. Mater. 27 (2015) 3789–3796.
- [33] A. Li, R.F. Lu, Y. Wang, X. Wang, K.L. Han, W.Q. Deng, Angew. Chem. Int. Ed. 49 (2010) 3330–3333.
- [34] K. Zhang, D. Kopetzki, P.H. Seeger, M. Antonietti, F. Vilela, Angew. Chem. Int. Ed. 52 (2013) 1432–1436.
- [35] X.H. Zhang, B.S. Peng, T.Y. Peng, L.J. Yu, R.J. Li, J. Zhang, J. Power Sources 298 (2015) 30–37.
- [36] X.H. Zhang, T.Y. Peng, L.J. Yu, R.J. Li, Q.Q. Li, Z. Li, ACS Catal. 5 (2015) 504–510.
- [37] J. Liu, C. Zhuang, K. Li, T. Peng, Phys. Chem. Chem. Phys. 17 (2015) 10944–10952.
- [38] T. Peng, X. Zhang, P. Zeng, K. Li, X. Zhang, X. Li, J. Catal. 303 (2013) 156–163.
- [39] X. Zhang, B. Peng, S. Zhang, T. Peng, ACS Sustainable Chem. Eng. 3 (2015) 1501–1509.
- [40] J.R. Ran, J. Zhang, J.G. Yu, M. Jaroniec, S.Z. Qiao, Chem. Soc. Rev. 43 (2014) 7787–7812.
- [41] H. Zhang, R.L. Zong, J.C. Zhao, Y.F. Zhu, Environ. Sci. Technol. 42 (2008) 3803–3807.
- [42] X. Ding, K. Zhao, L.Z. Zhang, Environ. Sci. Technol. 48 (2014) 5823–5831.